Solving (9) and (14) for $\langle\eta\rangle$ gives

$$\langle\eta\rangle=[1+2\langle n\rangle]^{-1}. \tag{17}$$

Substitution of (15) for $\langle n\rangle$ and solving for $\langle\eta\rangle$ gives

$$\epsilon_0\beta\langle\eta\rangle=\ln\left[\frac{1+\langle\eta\rangle}{1-\langle\eta\rangle}\right] \tag{18}$$

or

$$\tanh(\tfrac{1}{2}\alpha\langle\eta\rangle)=\langle\eta\rangle;\quad \alpha=NJ/k_BT \tag{19}$$

which is the exact result. The same result can be obtained from a general formalism given by Callen and Shtrikman[3] once it is known that $N^{-1}\sum_k\langle n\rangle$ can be written in the form

$$\frac{1}{N}\sum_k\langle n\rangle=[e^x-1]^{-1}, \tag{20}$$

where, in this case

$$x=\beta\epsilon_0\langle\eta\rangle. \tag{21}$$

At low temperatures (15) agrees, of course, with M. Bloch's approximation, which is

$$\langle n\rangle=[e^{\beta\epsilon(T)}-1]^{-1}, \tag{22}$$

$$\epsilon(T)=\epsilon_0[1-2\langle n\rangle]. \tag{23}$$

Therefore, using a Hartree-Fock termination, which in this case amounts to a Hartree approximation, on the G_2 function the exact result for $\langle\eta\rangle$ is obtained in terms of the boson distribution function (15).

ACKNOWLEDGMENTS

The author is indebted to Professor H. A. Gersch for bringing his attention to the problem treated here and for preliminary discussions.

[3] H. B. Callen and S. Shtrikman, Solid State Commun. 3, No. 1, 5 (1965).

PHYSICAL REVIEW VOLUME 141, NUMBER 1 JANUARY 1966

Photon Echoes*

I. D. Abella‡, N. A. Kurnit, and S. R. Hartmann†
Columbia Radiation Laboratory, Columbia University, New York, New York
(Received 3 August 1965)

Experiments are described in which a dilute ruby crystal is found to emit spontaneously a short pulse of light, the photon echo, at a time $\approx\tau_s$ after irradiation by two successive ruby-laser pulses separated by τ_s. The phenomenon is explained in terms of a macroscopic oscillating electric dipole moment, which is momentarily reformed at the time the photon echo is observed. The analysis predicts the echo polarization as well as the propagation direction relative to the input pulses. A necessary condition for obtaining echoes in ruby is the application of a moderate magnetic field close to the optic axis of the crystal, and a simple model based on Cr^{3+}—Al interactions is offered to account for this magnetic-field behavior. The relaxation time of the echo is found to exceed 250 nsec at 4.2°K but to be less than 70 nsec at 14°K, and is thought to be due to phonon-induced transitions in the excited $^2E(\bar{E})$ level. Multiple echo formation is also described.

I. INTRODUCTION

A SERIES of experiments have been reported which demonstrate the existence of photon echoes.[1,2] These and more recent experiments are now described in greater detail. A discussion of the theoretical considerations underlying the phenomenon of photon echoes is presented, and the predictions of this theory are compared with the experimental results.

The term photon echo is used in this paper to denote the pulse of light which is emitted spontaneously from a system of atoms previously irradiated by two coherent resonant light pulses and which is observed at a time after the second pulse very nearly equal to the time between the two excitation pulses. This nomenclature is suggested by the corresponding spin-echo[3] phenomenon observed in nuclear and electron-spin-resonance experiments.

The purpose of the first pulse is to excite a superradiant state[4] exhibiting an oscillating macroscopic electric dipole moment. This dipole moment quickly dephases because of inhomogeneous crystal-field strains, and the atoms then radiate at the normal spontaneous emission rate. The second excitation pulse reverses the dephasing process so that the system rephases at the

* This work was supported in part by the Army Research Office–Durham under Contract DA-31-124-ARO-D-224 and in part by the Joint Services Electronics Program under Contract DA-28-043 AMC-00099(E).

† Alfred P. Sloan Research Fellow.

‡ Present address: Dept. of Physics, University of Chicago.

[1] N. A. Kurnit, I. D. Abella, and S. R. Hartmann, Phys. Rev. Letters 13, 567 (1964); Bull. Am. Phys. Soc. 9, 658, 659 (1964).

[2] A published reference discussing the possibility of photon echoes was recently brought to the authors' attention: U. Kh. Kopvillem and V. R. Nagibarov, Fiz. Metal. i Metalloved. 15, 313 (1963).

[3] E. L. Hahn, Phys. Rev. 80, 580 (1950).

[4] R. H. Dicke, Phys. Rev. 93, 99 (1954).

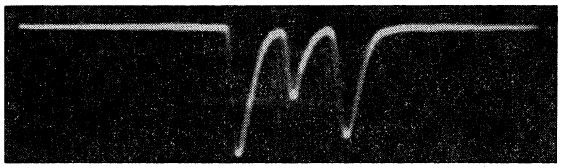

FIG. 1. The oscilloscope photograph shows output of photomultiplier which monitors radiation from the ruby sample. Time increases to the right and the scale is 50 nsec/div. The third pulse is the photon echo; the first two are the excitation pulses optically attenuated prior to detection.

same rate at which it dephased. When the rephasing process is complete, the macroscopic electric dipole moment is momentarily reformed, and the crystal emits an intense burst of light, the photon echo.

In Fig. 1 results are shown of a typical photon-echo experiment as performed with a ruby crystal excited by pulses from a ruby laser. The photograph shows three current pulses from a photomultiplier which monitors the radiation from the ruby sample. The two pulses on the left are the excitation pulses from the ruby laser while the third pulse is the photon echo. As will be explained later, the excitation pulses are greatly attenuated before reaching the photomultiplier, thereby preventing detector saturation, whereas the echo reaches the photomultiplier unattenuated.

Before proceeding to a detailed discussion of the various experiments which have been performed, a theoretical discussion will be presented, followed by a description of the apparatus used in the experiments.

II. THEORETICAL DISCUSSION

A. Equation of Motion

In the discussion of the photon-echo phenomenon, the crystal in which the photon echo is produced is considered to be made up of an ensemble of atoms which have just two states—the ground state and the excited state. The energy separation of these two states will be called $\hbar\Omega_0$, and it is assumed that an intense coherent source exists which produces radiation corresponding to this energy separation.

In discussions of the optical excitation of atoms in a crystal, it has been customary to describe the state of the system after an optical excitation simply by specifying the number of atoms in each energy state. This description is inadequate, however, since it does not take into account correlations between atoms, and it is these correlations which give rise to the photon echo. The present analysis includes correlations and proceeds in much the same way as the description of spin echoes, but there are important differences. In considering the production of spin echoes by precessing magnetic moments of nuclei or electrons, it is quite easy to give a physical picture of the behavior of the individual magnetic moments. There is a magnetic moment associated with both the ground and the excited states, and the net moment is visualized as precessing in the applied magnetic field. In the case of photon echoes in ruby, where the radiation is caused by an electric dipole transition, there is no corresponding electric dipole moment in either the ground or the excited states, and it is not obvious that one can form a picture of a precessing dipole moment as in the magnetic case. What the two systems have in common, however, is a matrix element of the corresponding dipole-moment operator between the ground and excited states, and this is enough to enable one to describe the formation of photon echoes in much the same way as spin echoes.[5]

One begins the analysis by considering a sample which is small compared with λ^3, where λ is the wavelength associated with the frequency Ω_0, i.e., $\lambda=2\pi c/\Omega_0$. The extension to larger volumes is straightforward and will be presented later. Consider the Hamiltonian given by

$$\mathcal{H}=\sum_j [\hbar\Omega_0 R_{j3}-\sqrt{2}P(E_x R_{j1}+E_y R_{j2})], \qquad (1)$$

where the notation of Dicke[4] has been used with the R_j operators operating on the jth atom and having the following properties:

$$\begin{aligned} R_{j1}[\cdots\pm\cdots]&=\tfrac{1}{2}[\cdots\mp\cdots],\\ R_{j2}[\cdots\pm\cdots]&=\pm\frac{i}{2}[\cdots\mp\cdots], \qquad (2)\\ R_{j3}[\cdots\pm\cdots]&=\pm\tfrac{1}{2}[\cdots\pm\cdots], \end{aligned}$$

where the + and − signs in the brackets refer to the atom being in the excited and ground states, respectively. The first term in Eq. (1) represents the energy of the system without any radiation present. The last two terms represent the interaction of the atoms with the applied radiation field (treated classically) from the laser. The quantities E_x and E_y are the transverse components of the electric field of the applied radiation field, while the constant P is given by $P=|\langle+,\ \mathbf{P}-\rangle|$, where $\mathbf{P}$ is the electric dipole moment operator. In this formulation, the z direction is the direction of propagation of the radiation. Since the sample size is small compared with λ^3, the spatial dependence of the radiation field can be neglected. The form of the Hamiltonian has been chosen so that an electric field of the form

$$E_x=E\cos\Omega t, \quad E_y=E\sin\Omega t, \qquad (3)$$

will cause transitions between the excited and ground states, whereas a radiation field of the opposite polarization will not. This choice of Hamiltonian is arbitrary, but the results obtained are general since other polarizations can be handled in the same way.

To describe the manner in which the excited atoms will radiate after being excited (if one neglects the weak incoherent spontaneous emission), it is necessary to determine how the transverse electric dipole moment of the system behaves as a function of time. This problem

[5] R. P. Feynman, F. L. Vernon, and R. W. Hellwarth, J. Appl. Phys. 28, 49 (1957); see also A. Abragam, *Principles of Magnetic Resonance* (Oxford University Press, London, 1961), p. 36.

is most easily solved by introducing another quantity, the pseudo-electric dipole moment, which behaves in a simple manner. The pseudo-electric dipole moment is defined by

$$\mathbf{p}=\sqrt{2}P\sum_j[R_{j1}\hat{x}+R_{j2}\hat{y}+R_{j3}\hat{z}]. \quad (4)$$

From the definitions of the R's and the Hamiltonian of the system, it is seen that the transverse components of $\mathbf{p}$ are the transverse components of the electric dipole moment. The z component of the expectation value of $\mathbf{p}$ does not yield the corresponding component of the electric dipole moment, since such a component does not exist, but gives instead a measure of the degree to which the system is excited. It is possible to express the Hamiltonian in a very simple form if a quantity $\mathcal{E}$ is defined as a pseudo-electric field:

$$\mathcal{E}=E_x\hat{x}+E_y\hat{y}-(\hbar\Omega_0/\sqrt{2}P)\hat{z}, \quad (5)$$

for then $\mathcal{H}$ is given by

$$\mathcal{H}=-\mathbf{p}\mathcal{E}. \quad (6)$$

To calculate the expectation value of $\mathbf{p}$, we use the relation

$$\langle\mathbf{p}\rangle=\mathrm{Tr}\rho\mathbf{p}, \quad (7)$$

where the density matrix ρ satisfies

$$\partial\rho/\partial t=-(i/\hbar)[\mathcal{H},\rho]. \quad (8)$$

From Eqs. (1)–(8) above, together with the commutation relations for the R_j's, i.e.,

$$[R_{j\alpha},R_{j'\beta}]=iR_{j\gamma}\delta_{jj'}\epsilon_{\alpha\beta\gamma}, \quad (9)$$

where $\epsilon_{\alpha\beta\gamma}$ is ±1 depending on whether $\alpha\beta\gamma$ is an even or odd permutation of the integers, and $\epsilon_{\alpha\beta\gamma}$ is zero when two or more indices are repeated, one finds

$$(d/dt)\langle\mathbf{p}\rangle=\gamma\langle\mathbf{p}\rangle\times\mathcal{E};\quad\gamma=\sqrt{2}P/\hbar. \quad (10)$$

The equation obtained has a very simple interpretation in that it describes a vector $\langle\mathbf{p}\rangle$ precessing about a field $\mathcal{E}$. This is to be compared with the equation of motion for the magnetization $\mathbf{M}$ in an applied field $\mathbf{H}$, i.e.,

$$(d/dt)\langle\mathbf{M}\rangle=\gamma_M\langle\mathbf{M}\rangle\times\mathbf{H}. \quad (11)$$

In the same way that the Bloch equations[6] are obtained for the magnetic case by adding relaxation terms, phenomenological relaxation terms can be added to Eq. (10) to obtain

$$\frac{d}{dt}\langle\mathbf{p}\rangle=\gamma\langle\mathbf{p}\rangle\times\mathcal{E}-\frac{\langle p_x\rangle\hat{x}}{T_2}-\frac{\langle p_y\rangle\hat{y}}{T_2}+\frac{[\langle p_0\rangle-\langle p_z\rangle]\hat{z}}{T_1}, \quad (12)$$

where T_2 and T_1 represent the transverse and longitudinal relaxation times, respectively. The quantity $\langle p_0\rangle$ is the thermal equilibrium value for the z component of $\langle\mathbf{p}\rangle$ which, for optical transitions, corresponds to all atoms being in the ground state. The quantity T_1 is normally the radiative lifetime of the excited state.

[6] F. Bloch, Phys. Rev. **70**, 460 (1946).

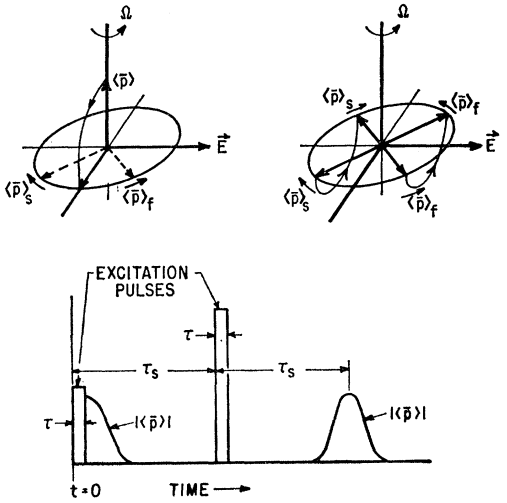

FIG. 2. (a) Vector diagram on left shows the result in the rotating frame of applying a 90° pulse to the pseudo electric dipole moment. (b) The diagram on the right shows the effect of applying a 180° pulse after a time τ_s. (c) Below is shown the time development of $|\langle\mathbf{p}\rangle|$.

B. Echo Formation

We are now in a position to present a simple description of how the photon echo is formed. The argument is similar to that used to explain spin echoes and is given here for completeness.[7]

Aside from relaxation effects the basic equation of motion is Eq. (10). When $\mathcal{E}_x=\mathcal{E}_y=0$, the vector $\mathbf{p}$ simply precesses about $\mathcal{E}_z$ at the frequency Ω_0, and it is advantageous to make a transformation of the form

$$(d/dt)\langle\mathbf{p}\rangle=(\partial/\partial t)\langle\mathbf{p}\rangle+\boldsymbol{\Omega}\times\langle\mathbf{p}\rangle \quad (13)$$

to enable us to observe the system in a frame of reference rotating at a frequency Ω. In this frame of reference, the equation of motion with $\mathcal{E}_x=\mathcal{E}_y=0$ becomes

$$(\partial/\partial t)\langle\mathbf{p}\rangle=\gamma\langle\mathbf{p}\rangle\times\{[\mathcal{E}_z+(\Omega/\gamma)]\hat{z}\}, \quad (14)$$

on setting $\boldsymbol{\Omega}=\Omega\hat{z}$. The quantity $\mathcal{E}_z$ is just $-\Omega_0/\gamma$. In this frame of reference, the rotating transverse electric field $\mathcal{E}=E(\hat{x}\cos\Omega t+\hat{y}\sin\Omega t)$ appears stationary, and so, in general,

$$(\partial/\partial t)\langle\mathbf{p}\rangle=\gamma\langle\mathbf{p}\rangle\times(\mathcal{E}_{z\,\mathrm{eff}}\hat{z}+E\hat{x}), \quad (15)$$

where an effective field $\mathcal{E}_{z\,\mathrm{eff}}$ has been defined as

$$\mathcal{E}_{z\,\mathrm{eff}}=\mathcal{E}_z+(\Omega/\gamma)=(-\Omega_0+\Omega)/\gamma. \quad (16)$$

This quantity is zero when $\Omega=\Omega_0$. It is possible to include the effect of crystalline field inhomogeneities by replacing Ω_0 with Ω_{0j} where Ω_{0j} varies slightly throughout the crystal. Each atom is then characterized by a different value of $\mathcal{E}_{z\,\mathrm{eff}}$ so that the different atoms will get out of phase once they are excited. This is similar to a transverse relaxation effect.

[7] H. Y. Carr and E. M. Purcell, Phys. Rev. **94**, 630 (1954).

To see how the photon echo is formed, consider the state illustrated in Fig. 2(a) in which the vector $\langle \mathbf{p} \rangle$ is directed along the z axis of a frame of reference which is rotating at the frequency $\boldsymbol{\Omega}$. At $t=0$ a pulse of radiation is applied so that E is no longer zero, and consequently, the vector $\langle \mathbf{p} \rangle$ precesses about the resultant field $\mathcal{E}_{z\,\mathrm{eff}}\hat{z} + E\hat{x}$. In the case where $E \gg \mathcal{E}_{z\,\mathrm{eff}}$, which we consider here, Eq. (15) requires that $\langle \mathbf{p} \rangle$ precesses about $E\hat{x}$. If the first pulse is applied for a time τ, where

$$\gamma E \tau = \pi/2, \tag{17}$$

then at $t=\tau$ the vector $\langle \mathbf{p} \rangle$ will have been rotated by 90° into the x-y plane. A pulse characterized by Eq. (17) is called a 90° pulse. As soon as the first pulse is turned off, the various $\langle \mathbf{p} \rangle$ vectors of the different atom groups will precess about their respective $\mathcal{E}_{z\,\mathrm{eff}}$ fields, and the net dipole moment will decrease. For simplicity we focus our attention on two atom groups, one labeled by f with $\mathcal{E}_{z\,\mathrm{eff}}$ positive, and one labeled s with $\mathcal{E}_{z\,\mathrm{eff}}$ negative. After a time τ_s each group will have precessed about $\mathcal{E}_{z\,\mathrm{eff}}$ by an angle $\theta = \gamma \mathcal{E}_{z\,\mathrm{eff}}(\tau_s - \tau)$, and in Fig. 2(a) the dotted vector lines refer to $\langle \mathbf{p} \rangle_f$ and $\langle \mathbf{p} \rangle_s$ at $t=\tau_s$. When $\langle \mathbf{p} \rangle_f$ and $\langle \mathbf{p} \rangle_s$ are no longer parallel, their vector sum will be decreased in magnitude, and consequently, the radiation from the system will decrease. At $t=\tau_s$ a second excitation pulse of length τ is applied so that the individual $\langle \mathbf{p} \rangle$ vectors again precess about the relatively strong radiation field E. When this second pulse is adjusted in amplitude so that $\gamma E \tau = \pi$, the effect of applying the pulse is as shown in Fig. 2(b). The precession of all $\langle \mathbf{p} \rangle$ vectors by π radians about $E\hat{x}$ is equivalent to a reflection about the x axis of all $\langle \mathbf{p} \rangle$ vectors lying in the x-y transverse plane. Since the application of this excitation pulse does not affect $\mathcal{E}_{z\,\mathrm{eff}}$, the individual $\langle \mathbf{p} \rangle$ vectors will continue to precess about $\mathcal{E}_{z\,\mathrm{eff}}$ after the second excitation pulse in the same sense and at the same angular velocity as just before the excitation pulse was applied. As a result the f and s groups (and all other groups) will then rephase in precisely the time taken by them to dephase. Figure 2(c) illustrates the time development of the magnitude of $\langle \mathbf{p} \rangle$ in relation to the excitation pulses. When the dipole moment has rephased, the spontaneous radiation will be increased, and the photon echo will be produced.

The state that has just been described and which exhibits a macroscopic electric dipole moment can be called a super-radiant state. This state radiates very strongly because of coherence and is made up of a linear combination of the super-radiant energy states of maximum "cooperation number," as defined by Dicke.[4] From Eq. (78) of Dicke's paper, one finds that the radiation from such a state is given by

$$I = \tfrac{1}{2}N(\tfrac{1}{2}N + \tfrac{1}{2})I_0, \tag{18}$$

where I_0 is the radiation intensity from a single isolated atom, and N is the number of atoms in the sample, which is small compared with λ^3. The quantity I is to be compared with the incoherent radiation intensity from the same sample

$$I_{\mathrm{inc}} = \tfrac{1}{2}NI_0. \tag{19}$$

From these considerations we can characterize the incoherent radiation as emanating from an ensemble of oscillating electric dipoles which are oscillating with random phases. The super-radiant state which gives rise to the photon echo is characterized by an ensemble of dipoles all oscillating in phase.

The above description of how the photon echo is obtained is easily extended to sample sizes large compared with λ^3. For large samples the spatial dependence of the radiation field must be taken into account, and therefore the components of the electric field at the jth atom must be given by

$$\begin{aligned} E_{xj} &= E\cos(\Omega t - kz_j), \\ E_{yj} &= E\sin(\Omega t - kz_j), \end{aligned} \tag{20}$$

so that Eq. (5) becomes

$$\mathcal{H} = -\textstyle\sum_j \mathbf{p}_j \cdot \boldsymbol{\mathcal{E}}_j. \tag{21}$$

From Eq. (7) the expectation value of the pseudo electric dipole moment is found to be

$$\begin{aligned} \langle \mathbf{p} \rangle = \mathrm{Tr}\rho^* \textstyle\sum_j [p_{zj}\hat{z} + (p_{xj}\hat{x} + p_{yj}\hat{y})\cos(\Omega t - kz_j) \\ + (p_{yj}\hat{x} - p_{xj}\hat{y})\sin(\Omega t - kz_j)], \end{aligned} \tag{22}$$

where ρ^* is defined by the transformation

$$\begin{aligned} \rho = \exp[-i\textstyle\sum_j R_{j3}(\Omega t - kz_j)]\rho^* \\ \times \exp[+i\textstyle\sum_j R_{j3}(\Omega t - kz_j)]. \end{aligned} \tag{23}$$

It is clear from the form of Eq. (22) that the vector defined by

$$\langle \mathbf{p}_j \rangle^* = \mathrm{Tr}\rho^* \mathbf{p}_j \tag{24}$$

describes the pseudo dipole moment as observed in a frame of reference rotating at the frequency Ω about the $\hat{z}$ direction. The equation of motion for $\langle \mathbf{p}_j \rangle^*$ is readily found to be given by

$$(d/dt)\langle \mathbf{p}_j \rangle^* = \gamma \langle \mathbf{p}_j \rangle^* \times \boldsymbol{\mathcal{E}}_j^*, \tag{25}$$

where $\boldsymbol{\mathcal{E}}_j^* = [(\Omega - \Omega_0)/\gamma]\hat{z} + E\hat{x}$ and $\gamma = \sqrt{2}P/\hbar$. One observes that when the sample volume is small compared with λ^3, Eq. (25) leads directly to Eq. (10).

The argument for the photon-echo formation now proceeds precisely as before, the only difference being in the character of the burst of radiation which is emitted by the phased oscillating dipole array. Since the sample is large, it acts as a large antenna, and its radiation can be highly directional.

The radiation intensity of the echo can be calculated classically by finding the radiation field from each dipole, summing over all dipoles, and then squaring. The result for a 90–180° pulse excitation is given by

$$I(\mathbf{k}) = \tfrac{1}{4}I_0(\mathbf{k},\mathbf{k}_z)[\textstyle\sum_j e^{i(\mathbf{k}-\mathbf{k}_z)\cdot\mathbf{r}_j}][\sum_l e^{-i(\mathbf{k}-\mathbf{k}_z)\cdot\mathbf{r}_l}], \tag{26}$$

where $I_0(\mathbf{k},\mathbf{k}_z)$ is the radiation intensity (for spontaneous radiation) in the direction $\mathbf{k}$ from a single atom which was excited by a burst of radiation in the $\hat{z}$ direction. When the sample is small compared with λ^3, the result is that $I(\mathbf{k})=(N/2)^2I_0(\mathbf{k},\mathbf{k}_z)$, but when the sample is large compared with λ^3, the exponential terms average to zero unless $\mathbf{k}\approx\mathbf{k}_z$.

Our considerations have been limited to the simple case in which the excitation pulses are parallel and have the same polarization. When these restrictions are relaxed, it is found that both the direction of propagation and the polarization of the echo are directly affected. In Appendix A the radiation intensity of the photon echo in the direction $\mathbf{k}$ due to excitation pulses with wave vectors $\mathbf{k}_1$ and $\mathbf{k}_2$ is found to be

$$I(\mathbf{k})=\tfrac{1}{4}N^2I_0|\{\exp[i(\mathbf{k}+\mathbf{k}_1-2\mathbf{k}_2)\mathbf{r}]\}_{\mathrm{av}}|^2, \quad (27)$$

where $\mathbf{k}_1$ refers to the first pulse and $\mathbf{k}_2$ refers to the second pulse. One notes that $I(\mathbf{k})$ will be maximum when

$$\mathbf{k}+\mathbf{k}_1-2\mathbf{k}_2=0, \quad (28)$$

and since the three k vectors are of equal magnitude, this requires that the excitation pulses be parallel. When the excitation pulses are not parallel, there will be interference effects, but these will be minimized when $\mathbf{k}$ is parallel to $2\mathbf{k}_2-\mathbf{k}_1$, i.e.,

$$\mathbf{k}=\eta(2\mathbf{k}_2-\mathbf{k}_1), \quad (29)$$

where η is a constant. The quantity $2\mathbf{k}_2-\mathbf{k}_1$ represents the wave vector of the excitation induced in the crystal, and it is clear from Fig. 3 that, if the second pulse makes an angle φ with respect to the first excitation pulse, then, for small angles φ, the photon echo will be propagated at an angle φ with respect to the second pulse. The wavelength λ^* of the excitation induced in the crystal is related to λ by

$$\lambda^*=\lambda(1-\varphi^2) \quad (30)$$

for small angles, and hence if φ is small enough to ensure that

$$l[(1/\lambda^*)-(1/\lambda)]\ll 1, \quad (31)$$

where l is the thickness of the crystal, then interference effects will be negligible.

The effect of using linearly polarized excitation pulses with different polarizations is analyzed in Appendix B. If the transition is a doublet with each component separately excited by orthogonal polarizations, the echo polarization will be simply related to the polarizations of the excitation pulses. It is found that, if the second pulse is plane polarized at an angle ψ with respect to the plane-polarized first pulse, then the echo will be plane polarized at an angle 2ψ with respect to the first pulse, i.e., an angle ψ with respect to the second pulse.

The practical advantages of the two results just stated are considerable since they enable one to separate the echo from the excitation pulses and thereby to prevent the detection apparatus from being overloaded.

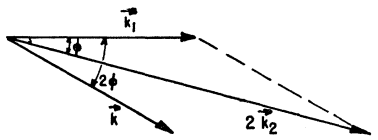

FIG. 3. Wave vectors showing the result of nonparallel excitation pulses. The echo is radiated in the direction $\mathbf{k}=2\mathbf{k}_2-\mathbf{k}_1$.

C. Numerical Estimates

Having discussed the theoretical basis for the photon-echo experiment, we shall now make numerical estimates of some of the more important parameters involved. The estimates will be made assuming the use of ruby as the material with which to perform the experiment.

The amount of laser power necessary for a 90° pulse is obtained from

$$\mathcal{P}=(c/4\pi)(\sqrt{\epsilon})E^2A, \quad (32)$$

where A is the area of the laser beam at the irradiated ruby crystal, and ϵ is the dielectric constant. Using Eqs. (10) and (17) together with[8]

$$W=64\pi^4(\sqrt{\epsilon})P^2/3\lambda^3h, \quad (33)$$

we find that

$$\mathcal{P}=\pi^4\epsilon c\hbar A/3\lambda^3\tau^2W. \quad (34)$$

The quantity W is the probability for an electric dipole radiation transition from the excited to the ground state. For ruby, $\sqrt{\epsilon}=1.76$

$$W\approx 2.5\times 10^2\ \mathrm{sec}^{-1},$$
$$\lambda\approx 6935\ \text{Å},$$

and the quantities A and τ were chosen to be

$$A=0.05\ \mathrm{cm}^2,$$
$$\tau=10^{-8}\ \mathrm{sec}.$$

Inserting these values into Eq. (34), we find that $\mathcal{P}\approx 2kW$. This power is quite small and easily obtained with any Q-switched ruby laser. Another parameter of interest is the concentration of Cr^{3+} ions in the Al_2O_3 matrix. This quantity is determined from the desirability of exciting all Cr^{3+} ions to the same degree. If $\mathcal{P}_{\mathrm{abs}}$ is the power that is absorbed in a 90° pulse by the Cr^{3+} ions, then the condition

$$\mathcal{P}_{\mathrm{abs}}=0.1\mathcal{P} \quad (35)$$

ensures relative uniformity of excitation throughout the crystal. The power absorbed is given by

$$\mathcal{P}_{\mathrm{abs}}=(\hbar\Omega)\left[\frac{1}{2}\frac{n}{2}(Al)\frac{T_2^*}{\tau}\right]\left(\frac{1}{\tau}\right), \quad (36)$$

where n is the number of Cr^{3+} ions/cm^3, l is the thickness of the crystal, and πT_2^* is the reciprocal inhomo-

[8] E. U. Condon and G. H. Shortley, *Theory of Atomic Spectra* (Cambridge University Press, Cambridge, England, 1959), p. 91, modified to include the dielectric constant.

geneous linewidth of the R_1 ruby line. Clearly, the power absorbed is given by the product of (1) the energy per photon absorbed ($\hbar\Omega$), (2) one-half (for a 90° pulse) the number of Cr^{3+} ions in the volume irradiated $\frac{1}{2}(nAl/2)$, the second factor of $\frac{1}{2}$ arising because (as will be shown in Sec. III) the laser used only overlaps with one half the ruby sample R line, (3) the fraction of Cr^{3+} ions which are excited (T_2^*/τ), and (4) ($1/\tau$). The factor (T_2^*/τ) appears because the pulse only excites the relatively few Cr^{3+} ions lying within the Fourier spectrum of the pulse, and this spectrum is narrow compared with the inhomogeneous linewidth. A second consequence of this selective excitation is that the width of the photon echo will be of the order of τ rather than T_2^*.

On combining Eqs. (34) through (36), we find

$$nl=\epsilon\pi^3/15\lambda^2WT_2^*, \tag{37}$$

and if we choose $l=0.1$ cm, and $T_2^*=10^{-10}$ sec based on a linewidth of 0.1 cm^{-1}, then

$$n=5\times10^{17}\ \text{atoms/cm}^3,$$

which is equivalent to a 0.002% doped ruby.

To obtain an estimate of the number of photons which are emitted in the echo, one can use either Eq. (26) or (27).

In Appendix C the expression for $I(\mathbf{k})$ is evaluated in the limit of a "short" radiator, in which case the radiation is confined to a solid angle,

$$\Delta\omega\approx\lambda^2/A \tag{38}$$

and the number of photons in the echo is given by

$$\mathfrak{N}\approx\frac{\tau}{\hbar\Omega}\int I(\mathbf{k})d\omega, \tag{39}$$

which can be expressed as

$$\mathfrak{N}=\left[\frac{1}{2}\frac{n}{2}\left(\frac{3\lambda^2 l}{8\pi\epsilon}\right)\frac{T_2^*}{\tau}\right]\left[\frac{1}{2}\frac{n}{2}(Al)\frac{T_2^*}{\tau}\right]W\tau. \tag{40}$$

The quantity $W\tau$ is the probability that an isolated atom will radiate during the time τ, while the factor in the second pair of brackets gives the number of atoms which are excited. As indicated in Eq. (18), when the sample is small compared with λ^3, the intensity of the radiation is proportional to the square of the number of atoms excited. For larger samples the radiation pattern becomes directional and the integrated radiation intensity does not increase as fast as it would for very small samples. As seen from Eq. (40), the volume of the sample (Al) has been replaced by an effective coherence volume ($3\lambda^2 l/8\pi\epsilon$) in the first pair of brackets to obtain the proper enhancement factor [cf. Eq. (C9)]. On evaluating $\mathfrak{N}$ using the parameters chosen previously, one finds that

$$\mathfrak{N}=3\times10^{11}\ \text{photons}.$$

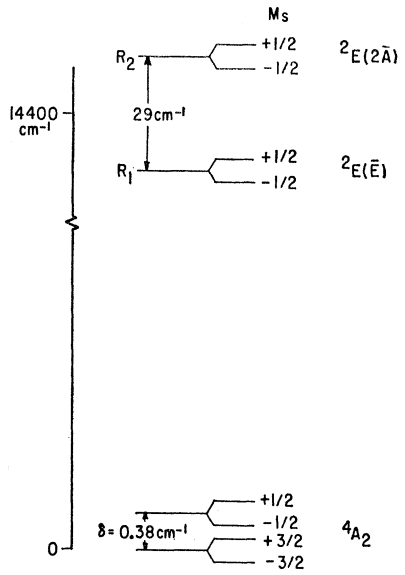

FIG. 4. Energy-level diagram of dilute ruby with the splitting shown for a weak magnetic field.

This quantity should be compared with the number of atoms which are excited by the first pulse, which is just 6×10^{12} excitations. Since the number of photons is much less than the number of excitations, we can expect that radiation damping effects are not very important.

The number of photons in the echo should also be compared with the number $\mathfrak{N}_B$ of incoherently radiated photons detected by the measuring apparatus in the time τ. This information gives the background noise and is easily obtained by replacing the first pair of brackets in Eq. (40) by an attenuation factor $\Delta\omega/4\pi$, the fractional solid-angle subtended by the detector. Estimating $\Delta\omega/4\pi$ to be 10^{-3}, we find

$$\mathfrak{N}_B=10^4\ \text{photons},$$

which is experimentally detectable, so that

$$\mathfrak{N}/\mathfrak{N}_B=3\times10^7$$

indicates the possibility of photon-echo observations with very large signal-to-noise ratios.

III. EXPERIMENTAL APPARATUS

The design of the photon-echo experiment with ruby as the working material was facilitated by the availability of ruby-laser techniques and a considerable body of relevant literature.[9–13] The essential elements of the photon-echo experiment consisted of (1) a ruby laser with suitable optical components from which two pulses of intense light could be obtained, (2) a ruby sample in

[9] O. Deutschbein, Ann. Phys. **14**, 712 (1932).
[10] S. Sugano and Y. Tanabe, J. Phys. Soc. Japan **13**, 880 (1958).
[11] F. J. McClung and R. W. Hellwarth, J. Appl. Phys. **33**, 838 (1962).
[12] E. O. Schultz-DuBois, Bell Sys. Tech. J. **38**, 271 (1959).
[13] A. L. Schawlow, *Advances in Quantum Electronics* (Columbia University Press, New York, 1961), p. 50.

which the echo is formed, and (3) a detector for observing the photon echo. Since the shortest practical pulses that could be produced by the laser were about 10 nsec in duration, the time scale of the experiment had a natural lower limit of about 50 nsec, which required a photon-echo lifetime of this order. The lifetime of the echo is determined by relaxation processes in the levels involved in the formation of the photon echo. In the case of ruby (Fig. 4 shows the energy-level diagram), the principal relaxation mechanisms in the $^2E(\bar{E})$ and $^4A_2$ states, which are the terminal levels for the R_1 laser transition, are strongly temperature-dependent.[14,15] The linewidth of the R_1 fluorescence increases from about 0.1 cm^{-1} at 77°K to 12 cm^{-1} at 300°K as a result of relaxation due to phonon-induced transitions in the $^2E(\bar{E})$ levels.[15] At 14°K this relaxation process appears to be the most important, and, based on the work of McCumber and Sturge[15] and Geschwind *et al.*[16] a photon-echo lifetime of about 100 nsec can be estimated. In order to allow a large safety factor, it was decided to keep the ruby sample at liquid-helium temperature, where relaxation times of the order of microseconds are expected.

Since the wavelengths of the absorption and laser R lines are temperature dependent,[9,17] it was necessary to choose a laser temperature which would permit overlap of the laser emission line with the absorption lines of the sample. Data of Schawlow[13] showed a small R_1 wavelength shift below 77°K, indicating that operating the laser at liquid-nitrogen temperature would allow appreciable overlap of the R_1 transitions of the sample and the laser. Such a feature would be considerably more convenient than the building of a liquid-helium-cooled laser.[18] To verify this possibility some high-resolution absorption measurements were carried out at low temperatures. A 3.4-m Jarrell-Ash spectrograph with photoelectric recording provided a resolution of about 0.05 Å. Some traces are shown in Fig. 5, and the results of wavelength measurements are tabulated. The important result to note is that the $^4A_2(M_s=\pm\frac{1}{2}) \rightarrow {}^2E(\bar{E})$ transition at 4.2°K essentially coincides with the $^4A_2(M_s=\pm\frac{3}{2}) \rightarrow {}^2E(\bar{E})$ transition at 77°K. The overlap is maintained even at liquid-hydrogen temperature so that in the range of interest below 20°K the upper of the two ruby ground-state transitions can be effectively pumped using a laser. Some degree of mismatch is possible, however, if the laser rod is appreciably heated during the flash.

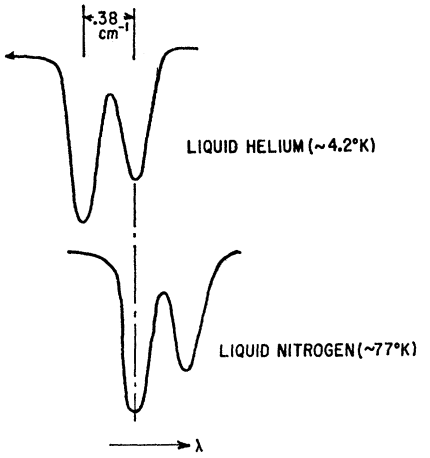

FIG. 5. High-resolution spectrograph traces of dilute ruby taken in absorption at two temperatures. The results are tabulated in Table I.

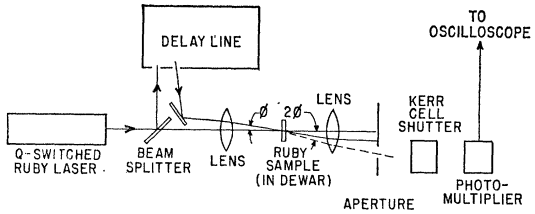

FIG. 6. Schematic diagram of experimental arrangement.

The experimental arrangement consisted of a Q-switched pulsed laser operating at liquid-nitrogen temperature, an optical delay line for producing the second pulse, a liquid-helium Dewar which held the sample and permitted external illumination, and detection apparatus. The schematic diagram is shown in Fig. 6.

The sample Dewar was a double helium Dewar with interchangeable tail sections. Windows of good quality sealed with indium O rings in the outer tail section allowed light to pass through with a minimum of distortion. The inner tail section was constructed of glass with glass windows and was connected to a stainless-steel flange via a glass-to-metal seal. Provisions were made for pumping the liquid helium down to 1.65°K. Operation below the λ point eliminated bubbling and significantly minimized scattered light. The crystal sample immersed in the liquid was supported by a lucite holder which could be rotated around a vertical axis passing through the sample. The latter was in the form of a polished disk 1 mm thick and 1 cm in diameter.

TABLE I. Table of R_1 wavelengths at low temperatures.

Temperature (°K)	$^4A_2(M_s\pm\frac{3}{2}) \rightarrow {}^2E(\bar{E})$ (Å)	$^4A_2(M_s\pm\frac{1}{2}) \rightarrow {}^2E(\bar{E})$ (Å)
2.2	6933.82	6934.00
20	6933.78	6933.96
77	6933.97	6934.15

[14] J. C. Gill, Proc. Phys. Soc. (London) **79**, 58 (1962).
[15] D. E. McCumber and M. D. Sturge, J. Appl. Phys. **34**, 1682 (1963).
[16] S. Geschwind, G. E. Devlin, R. L. Cohen, and S. R. Chinn, Phys. Rev. **137**, A1087 (1965).
[17] I. D. Abella and H. Z. Cummins, J. Appl. Phys. **32**, 1177 (1961).
[18] D. P. Devor, I. J. D'Haenens, and C. K. Asawa, Phys. Rev. Letters **8**, 432 (1962).

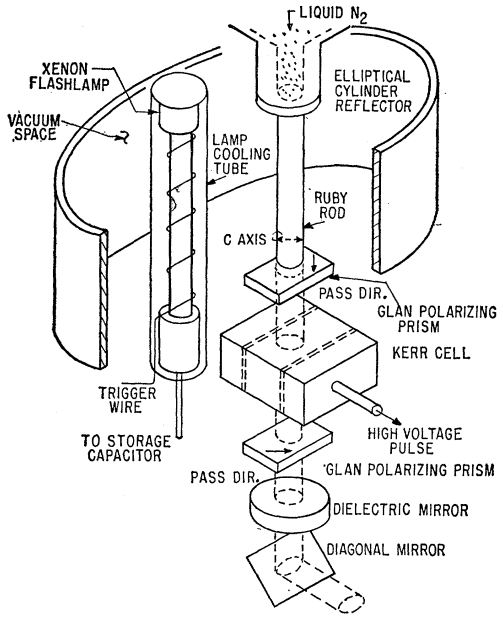

FIG. 7. View of ruby laser showing optical train used in Q switching.

In the initial experiments, the sample had a concentration of 0.005% Cr^{3+} by weight.[19] The optic axis was at an angle of about 15° with the normal to the disk and lay very nearly in the horizontal plane when mounted inside the Dewar. External to the Dewar were two pairs of water-cooled Helmholtz coils, with the ruby sample at their common center. One pair of coils provided a horizontal magnetic field of about ±350 G along the direction of the incident light, while the second pair provided an orthogonal field (also horizontal) of about ±200 G. Thus the effective field could be rotated in the horizontal plane around the same axis as the ruby-sample holder.

The ruby laser in this experiment was designed to be Q switched with a Kerr cell.[11] The difficulty of obtaining giant pulses at low temperatures is well known. The high gain at these temperatures tends to limit the energy storage in the rod and hence the pulse intensity. The tendency is for weak laser action to occur due to Fresnel reflection from various surfaces inside the laser cavity, even in the absence of a Kerr-cell activation pulse. This background laser oscillation could not be entirely suppressed. However, the use of crossed polarizing prisms largely prevented this light from leaving the laser. A Q-switched laser pulse was obtained nevertheless by triggering the Kerr cell in the cavity. The laser pulses averaged about 200-kW peak and were about 10–12 nsec in duration. A schematic design is shown in Fig. 7. The sapphire-clad ruby rod of length 2 in. and diameter ¼ in. is conduction cooled at one end by means of a copper clamp in contact with liquid nitrogen. The upper end of the rod is dielectric coated for greater than 99% reflection and is not in contact with the liquid nitrogen. The 90°, 0.05% Cr^{3+} rod is in the Dewar vacuum space and is excited by a linear flashtube using about 400 J/pulse. The output end is not coated, and light is coupled out through a Brewster window to the Kerr cell, which is between crossed polarizers, and then to the external 50% reflectivity mirror. The Kerr cell is pulsed into a half-wave condition and then off by a 20-nsec pulse-forming network, during which time the giant pulse is formed. The amount of low-level background laser light reaching the sample and detector is significantly reduced with this arrangement. The flashtube is cooled by passing boiled-off nitrogen gas through a surrounding glass tube. An elliptical focusing cylinder with end plates is used to collect the light efficiently. In order to avoid cycling the indium O rings used in the construction of the laser, the Dewar is continuously maintained at liquid-nitrogen temperature, and the system is kept under constant vacuum with a VacIon pump.

The required two pulses are obtained by dividing the beam with a beam-splitting mirror and subsequently recombining the two beams at the crystal sample. One beam is passed through an optical delay line in which the light is reflected a controllable number of times, and emerges identical to the first beam in pulse width and frequency spectrum. This delay is accomplished by means of a mirror arrangement originally used by White[20,21] for long-path infrared absorption experiments. The design is shown in Fig. 8. The concave mirrors are spaced by a distance equal to the radius of curvature (1.00 m) and thus recollimate the beam after each reflection. The particular advantage of this compact system is that the cross section of the beam does not increase with the number of reflections so that the nth beam is spatially separated from beams $n-1$ and $n+1$ at mirror C, thus avoiding ambiguities in the delay time. The mirrors were coated for high reflectivity

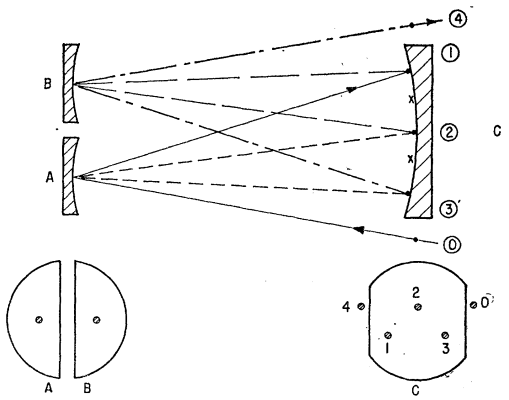

FIG. 8. Optical-delay-line design based on White cell (Refs. 20, 21).

[19] Photon echoes have also been obtained in crystals at concencentrations of 0.05 and 0.5%. It was found that the echo amplitude increased with the concentration.

[20] J. U. White, J. Opt. Soc. Am. **32**, 285 (1942).

[21] H. J. Bernstein and G. Hertzberg, J. Chem. Phys. **16**, 30 (1948).

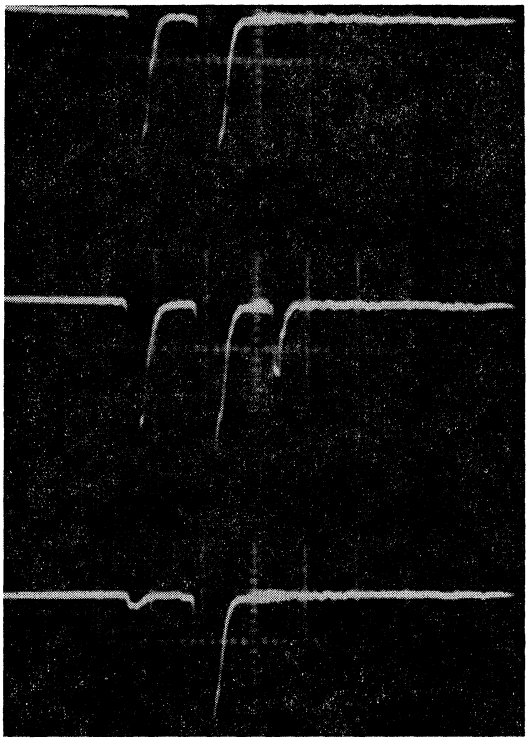

FIG. 9. Oscilloscope traces showing from the top, respectively, the effect without and with a magnetic field and of blocking the first pulse.

(99.5%) with dielectric films to reduce the reflection losses. The obtainable delay is limited by the loss of intensity and the decrease of beam separation with increasing n, and was about 140 nsec with the mirrors used in these experiments.

The light leaving the Dewar in the forward direction was collected with a lens and focused onto a photomultiplier. An aperture stop was placed, as shown in Fig. 5, to permit only the echo pulse to pass through. As is shown in Appendix A, and discussed previously, if the angular separation of the excitation pulses is φ, the echo will be emitted at an angle of 2φ with respect to the first pulse. The aperture stop was placed so as to block the first two pulses, and thereby to prevent overloading of the photomultiplier. In this experiment φ was about 3° and the aperture subtended an angle of $\approx 2°$.

The detection apparatus also employed a Kerr-cell shutter following the sample Dewar to reduce the background light scattered in the optical train and Dewar. A pulse opened this shutter for 100-nsec duration after the two excitation pulses were over, and thus permitted use of the high sensitivity of the photomultiplier during the time of the echo. The photomultiplier used was an RCA 7265, 14-stage tube with an S-20 cathode, terminated with 50-Ω coaxial cable and load. The output was displayed and photographed on a Tektronix 585 oscilloscope.

The light output of the Q-switched laser was tested for spectral and modal purity with an external Fabry-Perot interferometer. Several longitudinal modes, corresponding to a 20-cm cavity, were found to be present, and off-axis modes were also observed. However, no special precautions for mode selection were employed in these experiments.

IV. EXPERIMENTAL RESULTS

A. Detection of Echoes

With the experimental apparatus described in Sec. III, photon echoes were detected[1] (see Fig. 1), and a series of experiments was performed in order to verify the origin and the properties of the photon-echo signals. The tests can be roughly divided into two categories. One class of experiments involved changing the parameters associated with the sample alone, thereby localizing the effect to the ruby sample. The other set demonstrated that the detected pulse could not be attributed to some small fraction of the excitation laser pulses reflected from optical components of the system and delayed sufficiently to resemble a photon echo. Properties of the photon echo obtained from these and other experiments are largely consistent with the theory set forth earlier.

In order to observe photon echoes in ruby, a magnetic field must be applied to the sample. The photograph in Fig. 9 shows the effect on the echo amplitude with and without magnetic field. In this figure the pulse separation τ_s was 140 nsec, and the magnetic field directed along the optic axis of the sample was about 250 G. A detailed experimental description of this magnetic-field phenomenon together with an interpretation will be given later. It should be pointed out, however, that

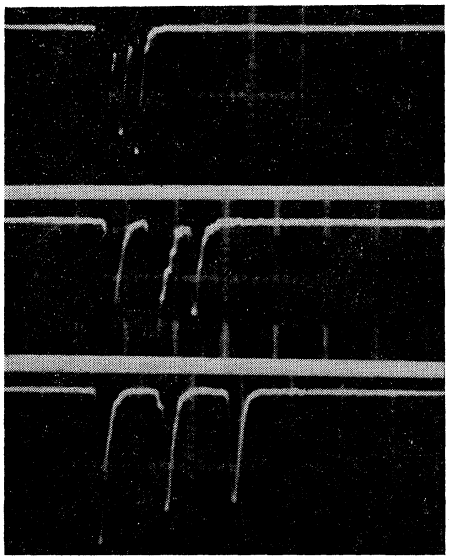

FIG. 10. Effect on echo of changing the delay times τ_s, respectively, 36, 83, and 137 nsec. The scale is 100 nsec/div.

the magnetic-field requirement is not a fundamental one, since the general theory applies in zero field. Therefore, it shall be implicit in the experimental descriptions which follow that a magnetic field of sufficient strength is applied to permit observation of the echo.

Figure 10 exhibits the necessary property of the echo —that of the dependence on the time separation of the two excitation pulses. The simple theory requires that the center of the echo occurs at a time $t=2\tau_s$ after the leading edge of the first pulse [see Fig. 2(c)]. This theory usually holds in the nuclear-resonance case, where the Fourier spectrum of the pulse applied to the sample is broader than the linewidth of the transition. In the case of pulses whose Fourier spectrum overlaps only a small fraction of the line, as is the case here for 10-nsec pulses and 0.1 cm^{-1} linewidth, the situation is more complicated. The observations showed that t exceeds $2\tau_s$ by about 5 nsec, independent of τ_s as measured on the oscilloscope photographs. Bloom[22] has shown that for inhomogeneous broadening in nuclear resonance, one expects an additional echo delay of $\tau/2$ or half the pulse width. Experiments performed with τ_s between 35 and 140 nsec are in good agreement with this theory, i.e., the echo maximum occurs at a time $t=2\tau_s+\tau/2$. Blocking one or the other of the excitation pulses resulted in the elimination of the echo (Fig. 9).

The photon echo was observed through a Kerr-cell shutter which was closed during the time of the excitation pulses (attenuation $\approx 10^{-3}$) and was opened immediately afterward. The echo was not observed if the shutter remained closed or if the shutter actuating pulse was shifted to a time after $t=2\tau_s+\tau/2$. This helped to eliminate the possibility that the observed echo was caused by spurious ion pulses in the photomultiplier, as well as to improve the detectability by preventing detector saturation.

The angle φ between the directions of the excitation pulses was 3°. As was previously stated and as shown in Appendix A, the photon echo is expected to be observed in a direction 2φ with respect to the first pulse. An aperture stop behind the crystal blocked the two excitation pulses from the detector, but allowed the echo to pass through. This aperture was moved around in a plane parallel to itself until the echo was maximum. The maximum was a broad one, but occurred at about the predicted angle of $2\varphi\approx 6°$.

The dependence of the echo intensity on the temperature of the ruby sample was tested. In the region of 1.65 to 4.2°K and $\tau_s=140$ nsec, no significant change of echo intensity was detected. Measurements above the λ point were complicated by scattering from bubbles in the liquid, making accurate comparisons difficult. The echo relaxation time at 4.2°K is conservatively estimated to be in excess of 250 nsec. The liquid helium was allowed to boil away, and the echo was subsequently observed for several minutes until the decreasing amplitude made it undetectable. Repeated attempts to observe the photon echo at hydrogen temperatures down to 14°K were unsuccessful with $\tau_s=75$ nsec. No significant temperature-tuning effects were expected, as described previously. The conclusion is that the echo depends on the ruby sample temperature and, that under the conditions of the experiment, is not observed above some as yet unknown temperature in the region of 4.2 to 14°K. The data are consistent with the phonon line-broadening theories,[15,23] which predict short relaxation time in this temperature region. An upper limit of ≈ 70 nsec was placed on the relaxation time at 14°K on the basis of this experiment.[24]

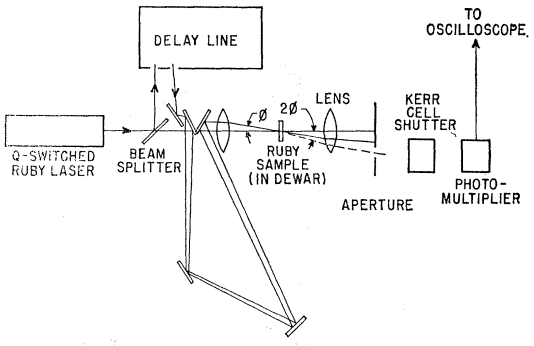

FIG. 11. Modified setup to test for spurious reflections.

The possibility of detecting a spurious reflection resembling an echo was analyzed with the arrangement shown in Fig. 11. The path lengths were increased by 2.5 m as shown. If a reflection from lenses or windows in the region of the Dewar retraced the delay line, the extra path length would be traversed twice. A consequence of this would be an increased delay of 17 nsec for the spurious "echo." However, no additional echo delay was observed with this arrangement. During the course of these experiments some small reflections were sometimes observed slightly delayed from the position of the echo, but these could be eliminated by adjustment of lenses and mirrors and careful diaphragming. These adjustments, however, had no effect on the photon echo itself. As an additional test, a Kerr cell placed in front of the Dewar was opened during the first two pulses and closed immediately following them. Thus any light reflected from components in the optical train would be attenuated when passing through this shutter at later times. However, no decrease in the photon-echo amplitude was observed with the Kerr cell in position.

The polarization dependence of the echo was also investigated. The laser output is normally plane polarized and by placing suitable wave plates and linear polarizers in each beam, the relative polarization of

[22] A. L. Bloom, Phys. Rev. 98, 1105 (1955).

[23] M. J. Blume, R. Orbach, A. Kiel, and S. Geschwind, Phys. Rev. 139, A314 (1965).

[24] See, however, results of N. A. Kurnit, I. D. Abella, and S. R. Hartmann, Proceedings of the Conference on the Physics of Quantum Electronics (to be published).

each of the two pulses could be varied. The polarization of the echo was determined with analyzers on the detection side of the Dewar.

When the two excitation pulses were plane polarized in the same direction, it was found that the echo was similarly polarized. However, when the second pulse was plane polarized at an angle ψ_0 with respect to the first, the predicted polarization of the echo (Appendix B) is at angle $2\psi_0$ with respect to the first pulse. Figure 12 shows the results of varying the analyzer with $\psi_0=45°$, with the theoretical curve $I=I_0\cos^2(\psi-2\psi_0)$ shown on the same figure. We note that the results are in good agreement. One advantageous outcome of this experiment was that by suitable selection of analyzer and polarizer angles, the second pulse could be almost entirely quenched before reaching the detector. This feature was important in experiments where τ_s was small and the echo would not otherwise be clearly distinguished from the preceding second pulse.

It is interesting to compare the echo intensity predicted in Sec. IIC with the observed intensities. The typical echo signal from a crystal of 0.005% Cr^{3+} concentration is observed to be about 5×10^8 photons. The calculated intensity corrected to this concentration is 2×10^{12} photons. Thus the observed signal is a factor of 4×10^3 smaller than expected.

There are a number of factors which can contribute to this. It had been assumed in making estimates that a single mode, 90°–180° pulse sequence was available. Since this is not the case experimentally, the resultant echo pulse is an average of a number of modes of differing and unknown intensity, to which the general result of Eq. (A18) must be applied. This could account for several orders of magnitude in echo signal. Also, since the two pulses are incident at angle φ to each other, interference effects are important and are properly calculated from Eqs. (27) and (A18). For $\varphi\approx3°$ in these experiments, the effective length of the crystal which contributes to the echo is $\approx l/10$, and the echo intensity could be reduced by 10^2. Laser-beam divergence due to focusing, and superposition error of the two pulses on the crystal tend to reduce the echo as well. It should be noted, in addition, that radiation damping effects mentioned previously could reduce the echo signal even at low Cr^{3+} concentration.

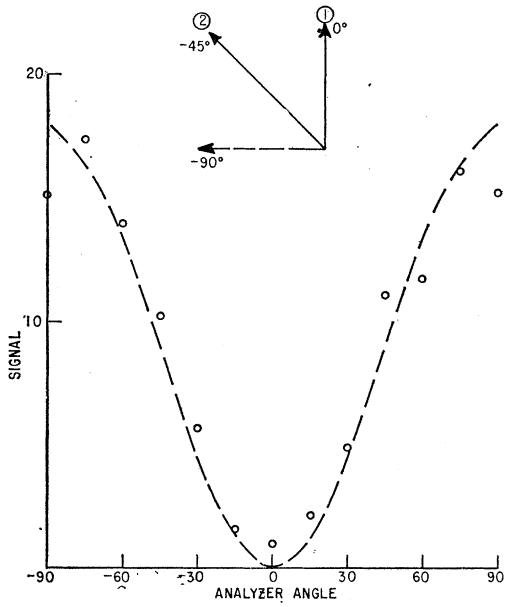

FIG. 12. Polarization dependence of echo. Excitation pulses are plane polarized at 90° to each other.

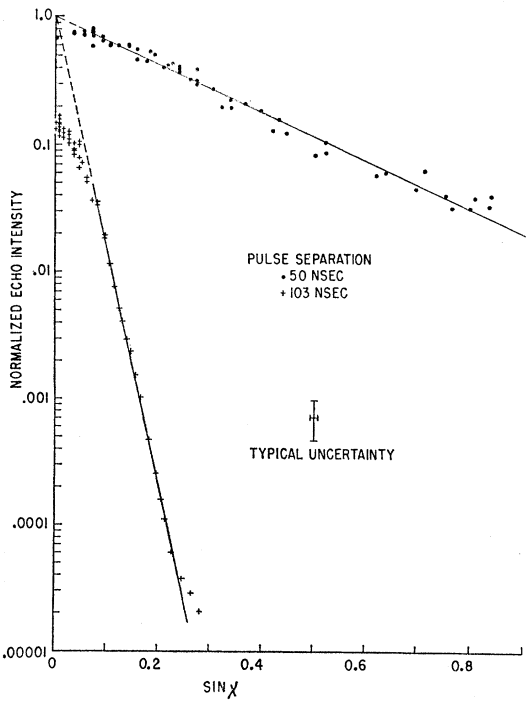

FIG. 13. Echo dependence on angular direction of magnetic field with respect to optic axis of sample for different values of τ_s. Each set of data is separately normalized.

B. Magnetic-Field Experiments

The fact that a magnetic field was necessary in the observation of photon echoes was an unexpected result of these experiments. The theory outlined in Sec. II showed that the incident light direction was sufficient to define an axis of quantization, and that echoes could occur in zero field. Initial experiments had shown that in addition to requiring a field of ≈50 G for $\tau_s=130$ nsec, the appearance of the photon echo was very sensitive to field direction with respect to the optic axis of the crystal. Maximum echo amplitudes were obtained when the field was parallel to the optic axis. When the optic axis was rotated by as little as 3° from this direction, the echo disappeared unless the magnetic field was correspondingly rotated. This field rotation was accomplished by adding some orthogonal field to

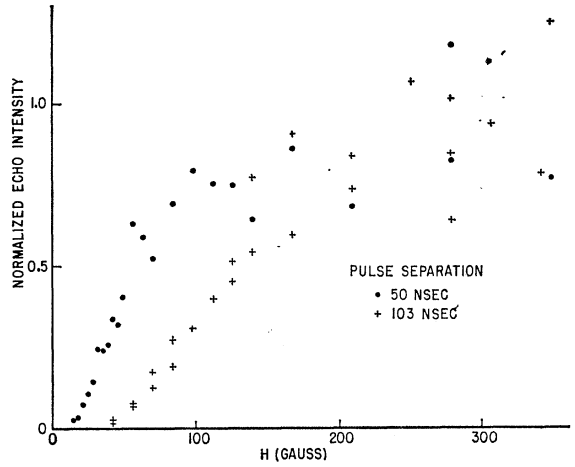

FIG. 14. Echo size versus magnetic field along optic axis.

the longitudinal field. These experiments were repeated for different values of τ_s. It was found that for smaller τ_s, the magnitude of the field required to observe echoes decreased, and the angular range over which this field could point increased.

Echo measurements were taken by fixing the crystal orientation and rotating the field direction $\chi=\tan^{-1}H_\perp/H_\parallel$. Some results are plotted in Figs. 13 and 14. The observations are summarized by noting that for fixed τ_s, there is an approximately simple exponential relation between echo size and field angle. The angular half-width is seen to decrease with increasing τ_s. Figure 13 shows curves for $\tau_s=50$ and 103 nsec. A graph of echo size versus magnitude of the field for different τ_s reveals that the minimum field necessary for observing an echo (when directed along the optic axis) decreases with decreasing τ_s as shown in Fig. 14.

The experimental results indicate that the magnetic field inhibits a relaxation process. A tentative explanation of this process is based on a classical model which attributes the echo relaxation to an internally modulated magnetic field at the Cr^{3+} sites,[25] which is due to a forced precession of the neighboring Al nuclei. This precession is believed to be caused indirectly by the change in state of the Cr^{3+} ion when excited by the laser pulse. The effect of the 90° excitation pulse is to reorient the electronic spin of the Cr^{3+} ion from alignment along the applied dc magnetic field to alignment in a direction approximately halfway between the directions of the applied field and the optic axis of the ruby. This reorientation arises from the anisotropy of the electronic g factors in the ground and excited states of ruby. Experimentally[12,26] the g factors are: $g[^4A_2]=1.99$ (essentially isotropic), while $g_\parallel[^2E(\bar{E})]=2.44$ (parallel to the optic axis), and $g_\perp[^2E(\bar{E})]\leq 0.1$ (perpendicular to the optic axis). Therefore, in the $^4A_2$ ground state the electronic spins are aligned parallel to the externally applied magnetic field, while in the $^2E(\bar{E})$ excited state, the alignment is essentially along the optic axis. After a 90° pulse, which results in a linear superposition of the wave functions of the two levels, the polarization direction is approximately halfway between the two directions. The reorientation of the Cr^{3+} electronic spin changes the direction of the effective magnetic field at neighboring Al sites, a field which arises from the large Cr-Al interaction.[27] As a result, the Al nuclei which were initially polarized in this field are now polarized at some angle to it and begin to precess around the new field direction. The precession of the Al nuclei modulates the magnetic field at the Cr^{3+} site, and there is a modulation of the level separation which degrades the amplitude of the photon echo. When the magnetic field is applied along the optic axis of the ruby, there is no pulse-induced reorientation, and the echo amplitude is maximum.

It should be noted that the reduction of the echo size as the applied field is reduced is also explained if one takes into account the local fields of about 12 G at the Cr^{3+} ion due to the Al nuclei.[27] The total magnetic field at the Cr^{3+} site is now the vector sum of the applied and local fields with the latter becoming more important as the external field decreases. Since the local field is random, the Cr^{3+} electrons are not aligned along the applied field and, on the average, are aligned at large angles to the optic axis. The echo in this case is degraded in the same fashion as described above.

This mechanism is presented here because it seems to account for the gross features of the magnetic field results: (a) that a magnetic field larger than local fields must be applied along the optic axis, (b) that for a fixed delay τ_s, the echo decreases with increased angle χ, and (c) that for a fixed χ, the echo decreases with increased τ_s. The model is also in accord with experimental results showing the independence of the field effect on temperature and Cr^{3+} concentration. However, calculations based on this model differ in important details from preliminary experimental results. At present, the difficulty is that the model does not directly account for the simple exponential dependence on angle χ which is found, and it suggests a half-width $\Delta\chi_{1/2}$ variation proportional to $1/\tau_s^2$, which cannot be verified with the data obtained thus far.

C. Multiple Echoes

We have also observed the phenomenon of multiple echos[28] from a ruby sample illuminated by two external pulses. The experimental modification necessary was to allow the angle between the directions of the incident

[25] The explanation given here is related to one given by L. G. Rowan, E. L. Hahn, and W. B. Mims, Phys. Rev. 137, A61 (1965) for the modulation of electron spin echoes.

[26] S. Geschwind, R. J. Collins, and A. L. Schawlow, Phys. Rev. Letters 3, 545 (1959).

[27] N. Laurance, E. C. McIrvine, and J. Lambe, J. Phys. Chem. Solids 23, 515 (1962).

[28] J. P. Gordon and K. D. Bowers, Phys. Rev. Letters 1, 368 (1958); Meir Weger, Ph.D. thesis, University of California, Berkeley, 1961 (unpublished).

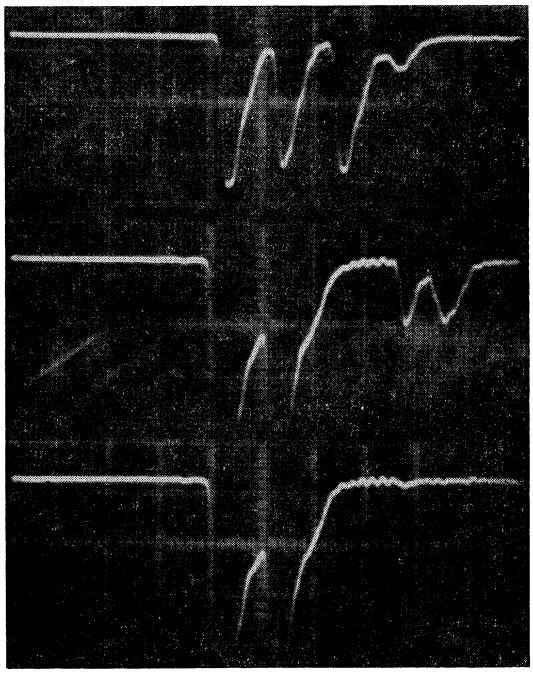

FIG. 15. Multiple echoes, using the two excitation pulses in same direction, observed with Kerr-cell shutter open for 100 nsec. Top trace shows first echo and small subsidiary pulse; middle trace has Kerr shutter opening delayed; last trace shows effect of removing the magnetic field.

pulses to be zero. It was previously shown that in this simple case, the echo is also radiated in the forward direction. The aperture-stop method of blocking the photomultiplier from direct illumination by the initial pulses was no longer available in this circumstance. However, an additional Kerr-cell shutter was placed in series with the existing one in front of the detector to attenuate the pulses further. Figure 15 shows the observation of multiple echoes. The top trace shows a small pulse after the echo. Since $\tau_s=50$ nsec here and one of the Kerr-cell shutters could remain open for only 100 nsec, the triggering of this shutter was delayed to permit observation of the multiple echo. Therefore, in the second trace, the first echo is not observed, but the second and third echoes are now visible. All the echoes disappeared when the magnetic field was removed. Multiple echoes can be understood if one considers an echo as a reorientation pulse when taken together with a pulse preceding it. Hence, the second echo is formed by considering the first echo and the second irradiating pulse as a pair, $\tau_s=50$ nsec, while the third echo can be formed in two ways: from the pair of first and second echoes, $\tau_s=50$ nsec, or from the pair of first excitation pulse and first echo, $\tau_s=100$ nsec. Since all these echoes are radiated at the same angle $\varphi=0$, they could all be observed. The earlier method of observation permitted detection of only the first echo because the multiple echoes would appear at progressively larger angles, 3φ and 4φ.

ACKNOWLEDGMENTS

We are pleased to acknowledge valuable discussions with R. Mieher, R. Novick, J. Giordmaine, and W. Blumberg. Useful conversations were also held with A. L. Schawlow, E. L. Hahn, A. M. Portis, and M. Weger. Thanks are due to the Columbia Radiation Laboratory machine shop for technical support. We would also like to thank A. G. Redfield for a critical reading of the manuscript and Viola M. Bennett for her editorial assistance.

APPENDIX A: DIRECTION OF ECHO PROPAGATION

To find the direction in which the photon echo is emitted after the system has been irradiated by two nonparallel pulses, it is convenient to use the following formalism of Dicke.[4] In an interaction representation, the effect of the radiation pulse on each atom is taken to be a rotation about some axis perpendicular to the number three axis in a pseudo "spin space"; the only difference between the effect of the pulse on each atom is in its arrival time. The effect of the pulse can, therefore, be represented by the unitary transformation

$$T=(\exp i\sum_{j=1}^{N}\Omega t_j R_{j3})\prod_{l=1}^{N}\exp i\frac{\theta}{2}(R_{l+}\alpha+R_{l-}\alpha^*)\times\exp(-i\sum_{j=1}^{N}\Omega t_j R_{j3}), \quad \text{(A1)}$$

where t_j is the arrival time of the pulse at the jth atom, $|\alpha|=1$, and the phase of α determines the direction of the rotation axis. If one sets $t_j=(1/\Omega)\mathbf{k}_1\cdot\mathbf{r}_j$, (A1) reduces to

$$T=\exp[i(\theta/2)(R_{\mathbf{k}_1+}\alpha+R_{\mathbf{k}_1-}\alpha^*)], \quad \text{(A2)}$$

where

$$R_{\mathbf{k}_1\pm}=\sum_{j=1}^{N}R_{j\pm}\exp(\pm i\mathbf{k}_1\cdot\mathbf{r}_j);\quad R_{j\pm}=R_{j1}\pm iR_{j2}. \quad \text{(A3)}$$

The density matrix in the interaction representation ρ^* is related to the density matrix in the Schrödinger representation by

$$\rho^*=\exp(i\Omega R_3 t)\rho\exp(-i\Omega R_3 t), \quad \text{(A4)}$$

and the equation of motion of the density matrix is given by

$$d\rho^*/dt-(i/\hbar)[\mathfrak{IC}^*,\rho^*], \quad \text{(A5)}$$

where

$$\mathfrak{IC}^*=\textstyle\sum_j \hbar\Delta\Omega_j R_{j3},\quad \Delta\Omega_j=\Omega-\Omega_{0j}. \quad \text{(A6)}$$

If at $t=0$ the density matrix is ρ_0, after the pulse it will be given by $\rho_1^*=T\rho_0 T^{-1}$. It is assumed that we may ignore $\mathfrak{IC}^*$ during the time of the pulse and neglect the pulse width with respect to the time between pulses. The density matrix then develops in time as

$$\rho^*(t)=\exp[-i\textstyle\sum_j\Delta\Omega_j t R_{j3}]\rho_1^*\exp[i\sum_j\Delta\Omega_j t R_{j3}]. \quad \text{(A7)}$$

If at $t=\tau_s$ one applies a θ'-degree pulse in the direction $\mathbf{k}_2$ and then lets the system again develop in time, the density matrix becomes

$$\rho^*=\mathcal{T}\rho_0\mathcal{T}^{-1}, \tag{A8}$$

where

$$\begin{aligned}\mathcal{T}=&\exp[-i\textstyle\sum_j\Delta\Omega_j(t-\tau_s)R_{j3}]\\&\times\exp[i(\theta'/2)(R_{\mathbf{k}_2+}\beta+R_{\mathbf{k}_2-}\beta^*)]\\&\times\exp[-i\textstyle\sum_j\Delta\Omega_j\tau_sR_{j3}]\\&\times\exp[i(\theta/2)(R_{\mathbf{k}_1+}\alpha+R_{\mathbf{k}_1-}\alpha^*)].\end{aligned} \tag{A9}$$

If ρ_0 is taken to be the density matrix corresponding to all the atoms being in the ground state,

$$\rho_0=\frac{1}{2^N}\prod_{l=1}^{N}(1-2R_{l3}), \tag{A10}$$

then (A6) becomes

$$\rho^*(t)=\frac{1}{2^N}\prod_l[1-(\mathcal{R}_l+\mathcal{R}_l^\dagger)], \tag{A11}$$

where

$$\begin{aligned}\mathcal{R}_l=&R_{l3}(\cos\theta\cos\theta'-\alpha\beta^*\\&\times\exp\{i[(\mathbf{k}_1-\mathbf{k}_2)\mathbf{r}_l-\Delta\Omega_l\tau_s]\}\sin\theta\sin\theta')\\&-iR_{l+}\alpha\exp[i(\mathbf{k}_1\mathbf{r}_l-\Delta\Omega_lt)]\sin\theta(1+\cos\theta')/2\\&-iR_{l+}\beta\exp\{i[\mathbf{k}_2\mathbf{r}_l-\Delta\Omega_l(t-\tau_s)]\}\cos\theta\sin\theta'\\&+iR_{l+}\alpha^*\beta^2\exp\{i[(2\mathbf{k}_2-\mathbf{k}_1)\mathbf{r}_l\\&-\Delta\Omega_l(t-2\tau_s)]\}\sin\theta(1-\cos\theta')/2.\end{aligned} \tag{A12}$$

As shown in Ref. 4, the radiation intensity in the direction $\mathbf{k}$ is given by

$$I(\mathbf{k})=I_0(\mathbf{k})\langle R_{\mathbf{k}+}R_{\mathbf{k}-}\rangle=I_0(\mathbf{k})\,\mathrm{Tr}R_{\mathbf{k}+}R_{\mathbf{k}-}\rho, \tag{A13}$$

where $I_0(\mathbf{k})$ is the radiation intensity of a single atom in the direction $\mathbf{k}$. Equation (A13) also holds with ρ replaced by ρ^* since R_3 commutes with $R_{\mathbf{k}+}R_{\mathbf{k}-}$. Hence

$$\begin{aligned}I(\mathbf{k})=&\frac{1}{2^N}I_0(\mathbf{k})\,\mathrm{Tr}R_{k+}R_{k-}\prod_l[1-(\mathcal{R}_l+\mathcal{R}_l^\dagger)]\\=&\frac{1}{2^N}I_0(\mathbf{k})\,\mathrm{Tr}\{\sum_j R_{j+}R_{j-}\prod_l[1-(\mathcal{R}_l+\mathcal{R}_l^\dagger)]\\&+\sum_j\sum_{m\neq j}R_{j+}R_{m-}\exp[i\mathbf{k}(\mathbf{r}_j-\mathbf{r}_m)]\\&\times\prod_l[1-(\mathcal{R}_l+\mathcal{R}_l^\dagger)]\}.\end{aligned} \tag{A14}$$

The term containing the double summation will give a contribution of the order of N^2 and is thus the term which leads to coherent spontaneous emission. If one now makes use of the relationships[4]

$$\begin{aligned}&\mathrm{Tr}A_iB_j=2^{-N}\,\mathrm{Tr}A_i\,\mathrm{Tr}B_j,\\&\mathrm{Tr}R_{j\alpha}=0,\quad\mathrm{Tr}R_{j\alpha}{}^2=2^{N-2},\quad\alpha=1,2,3,\end{aligned} \tag{A15}$$

this term becomes

$$\begin{aligned}&\frac{1}{2^{2N}}I_0(\mathbf{k})\sum_j\sum_{m\neq j}\mathrm{Tr}R_{j+}\mathcal{R}_j{}^\dagger\,\mathrm{Tr}R_{m-}\mathcal{R}_m\\&\times\exp[i\mathbf{k}(\mathbf{r}_j-\mathbf{r}_m)].\end{aligned} \tag{A16}$$

On substituting (A12) into (A16), one obtains a sum of terms which contain exponential factors of the form $\exp[i(\Delta\Omega_m-\Delta\Omega_j)f(t)]$. If one sets $t=2\tau_s$, then in the limit $\tau_s\gg\tau$, the only term which does not average to zero when summed over j and m is the one which arises from the product of the last term in (A12) with its Hermitian conjugate, for which $f(t)=t-2\tau_s=0$. It is, therefore, this term alone which gives rise to the photon echo. The second and third terms in (A12) similarly correspond to the super-radiant emission immediately after the first and second pulses, respectively.

Expression (A16) reduces to

$$\begin{aligned}&\tfrac{1}{4}I_0(\mathbf{k})\sum_j\sum_{m\neq j}\exp[i(\mathbf{k}+\mathbf{k}_1-2\mathbf{k}_2)(\mathbf{r}_j-\mathbf{r}_m)]\\&\times\sin^2\theta(1-\cos\theta')^2/4\end{aligned} \tag{A17}$$

which peaks at $\mathbf{k}=2\mathbf{k}_2-\mathbf{k}_1$. For small angles φ between $\mathbf{k}_2$ and $\mathbf{k}_1$, this yields the result that the echo is emitted at an angle $\approx 2\varphi$ with respect to $\mathbf{k}_1$ in the plane of $\mathbf{k}_1$ and $\mathbf{k}_2$.

The full expression for the radiation intensity at $t=2\tau_s$, including terms of order N, is, from (A14):

$$\begin{aligned}I(\mathbf{k})=&\tfrac{1}{2}NI_0(\mathbf{k})[1-\cos\theta\cos\theta'+\tfrac{1}{2}\sin^2\theta\tfrac{1}{4}(1-\cos\theta')^2\\&\times(N|\{\exp[i(\mathbf{k}+\mathbf{k}_1-2\mathbf{k}_2)\mathbf{r}]\}_{\mathrm{av}}|^2-1)],\end{aligned} \tag{A18}$$

where the average is taken over the position of all the atoms in the sample.

APPENDIX B: ECHO POLARIZATION

To find the echo polarization when the system is excited with two pulses polarized at an angle ψ with respect to one another, it is necessary to take into account that there are actually four levels of interest: the $(M_s=\pm\frac{1}{2})$ components of ${}^4A_2$, which, as explained earlier, are the only ground-state components that can be depopulated by a laser operated at nitrogen temperature, and the $(M_{s'}=\pm\frac{1}{2})$ components of ${}^2E(\bar{E})$. For an excitation field whose E vector is perpendicular to the optic axis, one observes only a σ^- transition which connects ${}^4A_2(M_s=+\frac{1}{2})$ with ${}^2E(\bar{E})(M_{s'}=+\frac{1}{2})$, and a σ^+ transition which connects ${}^4A_2(M_s=-\frac{1}{2})$ with ${}^2E(\bar{E})\times(M_{s'}=-\frac{1}{2})$.[10] If the relaxation times between the respective $(M=\pm\frac{1}{2})$ components are sufficiently long, our collection of four-level systems may be considered to be two independent collections of two-level systems, one of which responds to circularly polarized light of one sign and the other to circularly polarized light of the other sign.

A pulse linearly polarized at an angle ψ with respect to the x axis is represented by a field

$$\begin{aligned}\mathbf{E}&=2E_0(\hat{x}\cos\psi+\hat{y}\sin\psi)\cos\Omega t,\\&=E_0\{[\hat{x}\cos(\Omega t+\psi)+\hat{y}\sin(\Omega t+\psi)]\\&\quad+[\hat{x}\cos(\Omega t-\psi)-\hat{y}\sin(\Omega t-\psi)]\}.\end{aligned}\tag{B1}$$

We have for simplicity assumed a system small compared with λ^3 so that we may neglect the spatial variation of $\mathbf{E}$, but the results are easily generalized to a large system.

By Eq. (1) the interaction Hamiltonian is

$$\begin{aligned}\mathcal{H}_{\rm int}&=-\sqrt{2}PE_0[R^+(\Omega,\psi)+R^-(\Omega,\psi)]\\&=\mathcal{H}_{\rm int}{}^+ +\mathcal{H}_{\rm int}{}^-,\end{aligned}\tag{B2}$$

where

$$R^\pm(\Omega,\psi)\equiv R_1\cos(\Omega t\pm\psi)\pm R_2\sin(\Omega t\pm\psi).\tag{B3}$$

$\mathcal{H}_{\rm int}{}^+$ influences only the collection of two-level systems responding to right-hand circularly polarized radiation, whereas $\mathcal{H}_{\rm int}{}^-$ influences the other. We now consider the formation of an echo in one of these collections. It is convenient to transform to a rotating reference frame. Let

$$\begin{aligned}\mathcal{H}_{\rm int}{}^{+*}&=e^{i\Omega R_3 t}\mathcal{H}_{\rm int}{}^+e^{-i\Omega R_3 t}\\&=-\sqrt{2}PE_0e^{-i\psi R_3}R_1e^{i\psi R_3}.\end{aligned}\tag{B4}$$

The equation of motion of the transformed density matrix is given by (A5), where

$$\mathcal{H}^*=\sum_j\hbar\Delta\Omega_jR_{j3}+\mathcal{H}_{\rm int}{}^{+*},\quad\Delta\Omega_j=\Omega-\Omega_{0j}.\tag{B5}$$

A θ-degree pulse is applied at $t=0$, polarized at an angle $\psi=0$, followed by a θ'-degree pulse at $t=\tau_s$ polarized at an angle ψ. We assume for simplicity that the pulse is short enough so that its pulse spectrum is broad compared with the linewidth, and that the pulse length may be neglected compared with τ_s. The density matrix then becomes

$$\rho^*(t)=T\rho_0T^{-1},\tag{B6}$$

where

$$\begin{aligned}T=&\exp[-i\textstyle\sum_j\Delta\Omega_j(t-\tau_s)R_{j3}]\exp(-i\psi R_3)\exp(-i\theta' R_1)\\&\times\exp(i\psi R_3)\exp(-i\textstyle\sum_j\Delta\Omega_j\tau_sR_{j3})\exp(-i\theta R_1).\end{aligned}\tag{B7}$$

If the density matrix at $t=0$ is taken to be that corresponding to having all the atoms in the ground state,

$$\rho_0=\frac{1}{2^N}\prod_l(1-2R_{l3}),\tag{B8}$$

one obtains

$$\rho^*(t)=\frac{1}{2^N}\prod_l[1-2(\alpha_{l1}R_{l1}+\alpha_{l2}R_{l2}+\alpha_{l3}R_{l3})],\tag{B9}$$

where

$$\begin{aligned}\alpha_{l1}=&\sin\theta\sin(\Delta\Omega_l\tau_s-\psi)\cos[\Delta\Omega_l(t-\tau_s)+\psi]\\&+\cos\theta\sin\theta'\sin[\Delta\Omega_l(t-\tau_s)+\psi]\\&+\sin\theta\cos\theta'\cos(\Delta\Omega_l\tau_s-\psi)\sin[\Delta\Omega_l(t-\tau_s)+\psi],\\\alpha_{l2}=&\sin\theta\sin(\Delta\Omega_l\tau_s-\psi)\sin[\Delta\Omega_l(t-\tau_s)+\psi]\\&-\cos\theta\sin\theta'\sin[\Delta\Omega_l(t-\tau_s)+\psi]\\&-\sin\theta\cos\theta'\cos(\Delta\Omega_l\tau_s-\psi)\cos[\Delta\Omega_l(t-\tau_s)+\psi],\\\alpha_{l3}=&\cos\theta\cos\theta'-\sin\theta\sin\theta'\cos(\Delta\Omega_l\tau_s-\psi).\end{aligned}\tag{B10}$$

Hence

$$\langle R_i\rangle^*=\mathrm{Tr}R_i\rho^*=-\tfrac{1}{2}\textstyle\sum_l\alpha_{li}.\tag{B11}$$

Under the assumption that τ_s is sufficiently great so that $\sum_l\sin\Delta\Omega_l\tau_s=\sum_l\cos\Delta\Omega_l\tau_s=0$, $(1/N)\sum_l\cos^2\Delta\Omega_l\tau_s=\frac{1}{2}$, Eq. (B11) reduces, at $t=2\tau_s$, to

$$\begin{aligned}\langle R_1\rangle^*&=\tfrac{1}{2}N(\sin2\psi\sin\theta)(1-\cos\theta')/2,\\\langle R_2\rangle^*&=-\tfrac{1}{2}N(\cos2\psi\sin\theta)(1-\cos\theta')/2.\end{aligned}\tag{B12}$$

The transverse component of the expectation value of $\mathbf{p}$ therefore makes an angle of $\pi/2+2\psi$ with respect to the $\hat{x}$ axis in this rotating reference frame (θ is taken to be negative in accordance with the sign of $\mathcal{H}_{\rm int}$). This result is quite easily visualized by the use of a vector model in the case of a 90° pulse followed by a 180° pulse. It was previously obtained by Hahn[3] for two 90° pulses. The above analysis shows it to be true for arbitrary θ and θ'.

A similar analysis for the other collection of two-level systems shows that the transverse component of the expectation value of $\mathbf{p}$ makes an angle of $-\pi/2+2\psi$ with respect to the $\hat{x}$ axis of a frame rotating in the opposite sense to the one considered above. The resultant of these two oppositely rotating dipole moments gives a linear oscillating dipole moment which makes an angle 2ψ with the $\hat{x}$ axis of the laboratory frame. The emitted radiation is therefore polarized at an angle of 2ψ with respect to the $\hat{x}$ axis.

APPENDIX C: INTENSITY OF ECHO RADIATION

The radiation intensity in the direction $\mathbf{k}$ from a system which has been excited by 90° and 180° pulses with wave vector $\mathbf{k}_1$ is given by Eq. (A18).

$$I(\mathbf{k})=I_0(\mathbf{k})\tfrac{1}{4}N\{N|[\exp i(\mathbf{k}_1-\mathbf{k})\mathbf{r}]_{\rm av}|^2+1\},$$

where the average is taken over the positions of all the atoms, $I_0(\mathbf{k})$ is the radiation intensity of an isolated atom in the direction $\mathbf{k}$, and N is the total number of atoms. For large N we may neglect the term of order N relative to the term of order N^2, and we have for the radiation intensity integrated over all angles

$$S=\tfrac{1}{4}N^2\int\int I_0(\mathbf{k})|[\exp i(\mathbf{k}_1-\mathbf{k})\mathbf{r}]_{\rm av}|^2d\Omega.\tag{C1}$$

For a cubic array of $N=N_xN_yN_z$ atoms of spacing a,

$$|[\exp i(\mathbf{k}_1-\mathbf{k})\mathbf{r}]_{\mathrm{av}}|^2 = \frac{1}{N^2}\prod_{i=x,y,z}\left[\frac{\sin^2(\mathbf{k}_1-\mathbf{k})_iN_i(a/2)}{\sin^2(\mathbf{k}_1-\mathbf{k})_i(a/2)}\right]. \quad \text{(C2)}$$

For convenience N_y is set equal to N_x, so that the radiating sample is a rectangular parallelepiped of side $2s=N_xa$, area $A=4s^2$, and length $l=N_za$. For a sample large compared with λ^3, expression (C1) peaks sharply at $\mathbf{k}=\mathbf{k}_1$, and almost all of the radiation is confined to the major lobe of the radiation pattern. In the limit of large Fresnel number, $s^2/\lambda l\gg 1$, the first zero in the radiation pattern is determined solely by the width of the sample. It then becomes possible to remove the N_z dependence from the integral and treat the problem by the standard methods for a broadside array.[29,30] In order to do the integration, it is most convenient to use the polar coordinates adopted by Slater,[30] with $\mathbf{k}_1$ along the z axis:

$$\begin{aligned}(\mathbf{k}_1-\mathbf{k})_x&=-k\cos\theta,\\ (\mathbf{k}_1-\mathbf{k})_y&=-k\sin\theta\sin\varphi,\\ (\mathbf{k}_1-\mathbf{k})_z&=k(1-\sin\theta\cos\varphi).\end{aligned} \quad \text{(C3)}$$

The radiation peaks in the direction $\theta=\frac{1}{2}\pi$, $\varphi=0$, and the first zeros in the radiation pattern occur when either $\frac{1}{2}\pi-\theta$ or φ are equal to $2\pi/N_xka$. It is then a good approximation to set $\sin\theta=1-[\frac{1}{2}(\frac{1}{2}\pi-\theta)^2]\approx 1$, $\cos\theta=\frac{1}{2}\pi-\theta$, $\sin\varphi=\varphi$, $\cos\varphi=1-(\frac{1}{2}\varphi)^2$. Thus,

$$S\approx\tfrac{1}{4}\int_{-2\pi/N_xka}^{2\pi/N_xka}\int I_0(\mathbf{k}_1)F(\theta,\varphi)d(\tfrac{1}{2}\pi-\theta)d\varphi, \quad \text{(C4)}$$

where

$$F(\theta,\varphi)=\frac{\sin^2[\frac{1}{2}N_xka(\frac{1}{2}\pi-\theta)]}{\sin^2[\frac{1}{2}ka(\frac{1}{2}\pi-\theta)]}\frac{\sin^2[\frac{1}{2}N_xka\varphi]}{\sin^2[\frac{1}{2}ka\varphi]} \times\frac{\sin^2[\frac{1}{2}N_zka(\frac{1}{2}(\frac{1}{2}\pi-\theta)^2+\frac{1}{2}\varphi^2)]}{\sin^2[\frac{1}{2}ka(\frac{1}{2}(\frac{1}{2}\pi-\theta)^2+\frac{1}{2}\varphi^2)]}. \quad \text{(C5)}$$

In the limit of large Fresnel number, the last factor in $F(\theta,\varphi)$ is well approximated by replacing the sines by their arguments, yielding just N_z^2. The integrals may then be approximated by extending the limits of integration to $\pm\infty$:

$$\begin{aligned}S&\approx\tfrac{1}{4}I_0(\mathbf{k}_1)N_z^2N_x^2\frac{\lambda^2}{\epsilon\pi^2a^2}\left[\int_{-\infty}^{\infty}\frac{\sin^2\xi}{\xi^2}d\xi\right]^2 \quad \text{(C6)}\\ &=\tfrac{1}{4}I_0(\mathbf{k}_1)N^2(\lambda^2/\epsilon A).\end{aligned}$$

This is to be compared with the incoherent rate for a system of N atoms, half of which are excited:

$$S_{\mathrm{inc}}=\tfrac{1}{2}N\int_0^{2\pi}d\varphi\int_0^{\pi}I_0(\mathbf{k}_1)\sin^2\theta\sin\theta\,d\theta, \quad \text{(C7)}$$

where the factor $\sin^2\theta$ gives the radiation pattern for a linear dipole oscillator.[8] This yields

$$S_{\mathrm{inc}}=\tfrac{1}{2}NI_0(\mathbf{k}_1)(8\pi/3). \quad \text{(C8)}$$

Hence

$$S\approx\tfrac{1}{2}N(3\lambda^2/8\pi\epsilon A)S_{\mathrm{inc}}. \quad \text{(C9)}$$

Similarly one obtains, in the limit of small Fresnel number,

$$S\approx\tfrac{1}{2}N\left(\frac{3}{8}\frac{\lambda}{(\sqrt{\epsilon})l}\right)S_{\mathrm{inc}}. \quad \text{(C10)}$$

[29] J. A. Stratton, *Electromagnetic Theory* (McGraw-Hill Book Company, New York, 1941), p. 443.
[30] J. C. Slater, *Microwave Transmission* (McGraw-Hill Book Company, New York, 1942), p. 256 *et seq.*

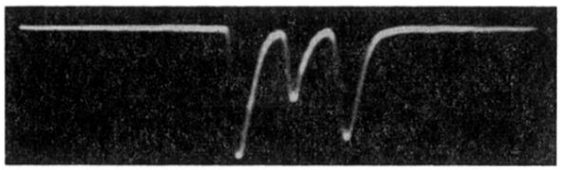

FIG. 1. The oscilloscope photograph shows output of photomultiplier which monitors radiation from the ruby sample. Time increases to the right and the scale is 50 nsec/div. The third pulse is the photon echo; the first two are the excitation pulses optically attenuated prior to detection.

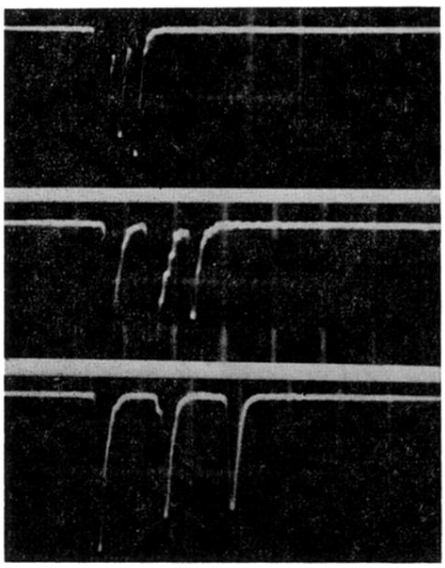

FIG. 10. Effect on echo of changing the delay times τ_s, respectively, 36, 83, and 137 nsec. The scale is 100 nsec/div.

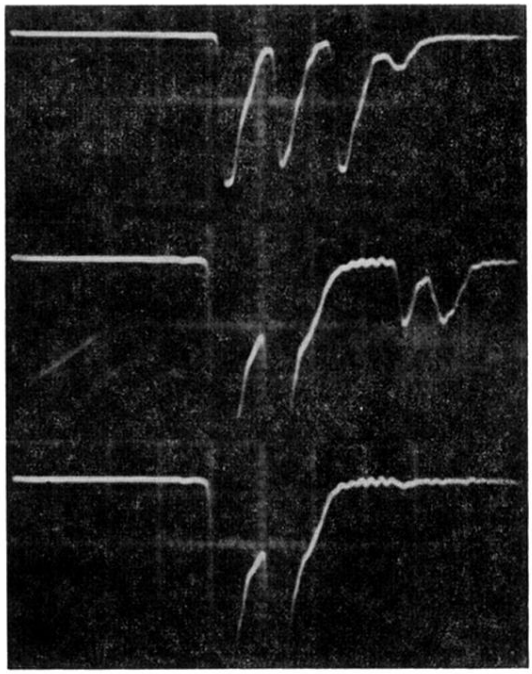

FIG. 15. Multiple echoes, using the two excitation pulses in same direction, observed with Kerr-cell shutter open for 100 nsec. Top trace shows first echo and small subsidiary pulse; middle trace has Kerr shutter opening delayed; last trace shows effect of removing the magnetic field.

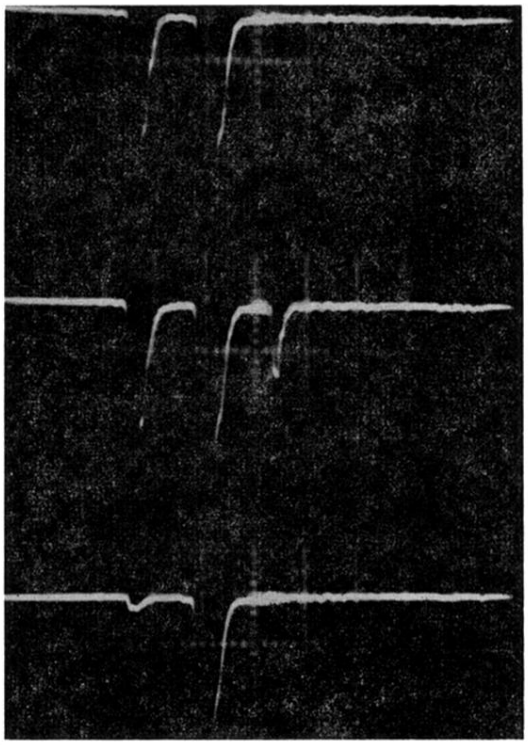

FIG. 9. Oscilloscope traces showing from the top, respectively, the effect without and with a magnetic field and of blocking the first pulse.